Multiple phase rifting and subsequent inversion in the West Netherlands Basin: implications for geothermal reservoir characterization

Annelotte Weert[1], Kei Ogata[1], Francesco Vinci[2], Coen Leo[3], Giovanni Bertotti[4], Jerome Amory[2], Stefano Tavani[1,5]

[1]Department of Earth, Environmental and Resource Sciences (DiSTAR), University of Naples 'Federico II', Naples, 80126, Italy
[2]PanTerra Geoconsultants B.V., Leiderdorp, 2352BZ, The Netherlands
[3]Geoleo B.V. Consultancy, The Hague, 2596PL, The Netherlands
[4]Faculty of Civil Engineering and Geosciences, Technical University of Delft, Delft, 2628CN, The Netherlands
[5]Consiglio Nazionale delle Ricerche, IGAG, Rome, 00185, Italy

Correspondence to: Annelotte Weert (annelotteweert@gmail.com)

Abstract. Aiming to contribute to the energy transition, this study provides an integrated picture of the geothermal system hosted in the West Netherlands Basin and shows how the reconstruction of the basin's geological history can contribute to the correct exploitation of its geothermal resources. In the West Netherlands Basin, the main geothermal targets are found in the Cretaceous and Jurassic strata that were deposited during rifting and post-rifting stages and were deformed during the subsequent basin inversion. Despite multiple studies on the tectonic setting, the timing and tectono-stratigraphic architecture of the rift system and its overall control on geothermal systems are still to be fully deciphered. In this framework, a detailed interpretation of the syn- and post-rift intervals in the West Netherlands Basin will be given within the framework of geothermal exploration. With a renewed interpretation of a recently released and reprocessed seismic 3D cube, covering a large portion of the onshore section of the basin, we identified two important Jurassic rifting episodes and one Late Cretaceous inversion event. These two Jurassic rifting phases not only created sedimentary accommodation, but also caused compartmentalisation of the depocenters of the Late Jurassic Nieuwerkerk Formation, which is the main regional producing geothermal target. Accordingly, the central portions of the half-grabens show good potential for geothermal exploration.

1 Introduction

Subsurface fluid flow systems hosted in rift basins form part of the resources that are indispensable in the global challenge to cut greenhouse gas emissions and cover current and future needs with sustainable energy sources. Basins' bounding faults and the laterally and vertically varying characteristics of sedimentary basins' fills control the distribution, abundance and recoverability of these resources (Gawthorpe and Leeder, 2000), including the heat flow needed for high (T > 150°C) to low (T < 90°C) enthalpy geothermal systems (Carapezza et al., 2022). As a frontrunner in Europe, the Netherlands recognizes the

contribution of geothermal energy to be crucial for a successful energy transition (e.g. Kramers et al., 2012; Willems and Nick, 2019; Mijnlieff, 2020).

The West Netherlands Basin (WNB) (Fig. 1a) is a former prosperous hydrocarbon province where the interest changed to geothermal energy in the past decade. Having an energy-demanding greenhouse horticulture, a dense population, which includes the cities of Rotterdam and The Hague, and an average geothermal gradient of 31°C km^{-1} (Bonté et al., 2012), the WNB is considered as one of the best case studies for low-enthalpy geothermal exploration (Kramers et al., 2012; Crooijmans et al., 2016; Willems et al., 2017c; Willems, 2017; Vondrak et al., 2018; Willems and Nick, 2019; Willems et al., 2020; Boersma et al., 2021). A typical geothermal project in the Netherlands comprises a low-enthalpy geothermal system for direct heat that contains two or more wells; hot water is produced by production wells and re-injected by injection wells after the heat has been extracted (Limberger et al., 2018). In the WNB, only open loop geothermal systems (i.e. a geothermal doublet that uses the aquifer as heat exchanger) reaching production temperatures ranging from 70°C to 90°C are used (Willems et al., 2017b). With the hydrocarbon exploitation in the WNB, an extensive data collection was gathered (e.g. seismic and well data), publicly available at nlog.nl (e.g. Duin et al., 2006; Kombrink et al., 2012). Up to 2023, 14 geothermal projects were realised in the area (Geothermie Nederland, 2023), targeting aquifers hosted by the post-rift Cretaceous Rijnland Group (two projects), syn-rift Jurassic Nieuwerkerk Formation (ten projects) and pre-rift Triassic Buntsandstein (two projects). Financial budgets for geothermal projects are much tighter than for traditional hydrocarbon exploration, making the successful delivery of every well essential to ensure the economic profitability of the geothermal projects. Understanding how the tectonic evolution of a rift basin influences the key parameters used for planning geothermal wells is therefore critical. Such parameters include aquifer thickness and heterogeneity. A thicker and more homogeneous reservoir is preferred, as it allows for better fluid flow, a higher heat extraction and an increased heat recovery (Crooijmans et al., 2016; Willems et al., 2017b), therefore making a geothermal system more profitable. As noted by Willems et al. (2020), current geothermal projects in the WNB demonstrate that the aquifer geology is still not fully understood. Increased knowledge of the regional architecture of the sedimentary rocks hosting aquifers, sub-seismic structural geology, and aquifer properties such as stratigraphic architecture, thickness and heterogeneity, would help to de-risk the geothermal well planning in the area (Willems et al., 2020).

Presently, the main target for geothermal exploration in the WNB is the Jurassic Nieuwerkerk Formation (Willems et al., 2017c; Vondrak et al., 2018). This formation was interpreted as deposited in a fluvial-deltaic environment during the main rifting phase that shaped the basin, resulting in sharp lateral thickness and facies variations (van Wijhe, 1987; den Hartog Jager, 1996; Willems et al., 2020). Subsequent basin inversion caused uplift and deformation within the Nieuwerkerk Formation(e.g. van Wijhe, 1987; van Balen et al., 2000; de Jager, 2003; Deckers and van der Voet, 2018). This tectonic history makes the reconstruction of the Jurassic tectono-sedimentary sequence, and therefore the thickness of its reservoir rocks more complex.

The quality of the recently reprocessed and released L3NAM2012AR seismic 3D cube allows a detailed reconstruction of the main subsurface structures. Contrasting to previous studies that mainly focussed on the NW-part of the onshore WNB (e.g. DeVault and Jeremiah, 2002; Willems et al., 2017c; Vondrak et al., 2018), now the SE-part of the onshore WNB could be

65 integrated into the study area as well. Accordingly, this study gives a detailed overview of the sub-seismic structural geology and increases the knowledge of the regional aquifer architecture, with a focus on the Nieuwerkerk Formation.
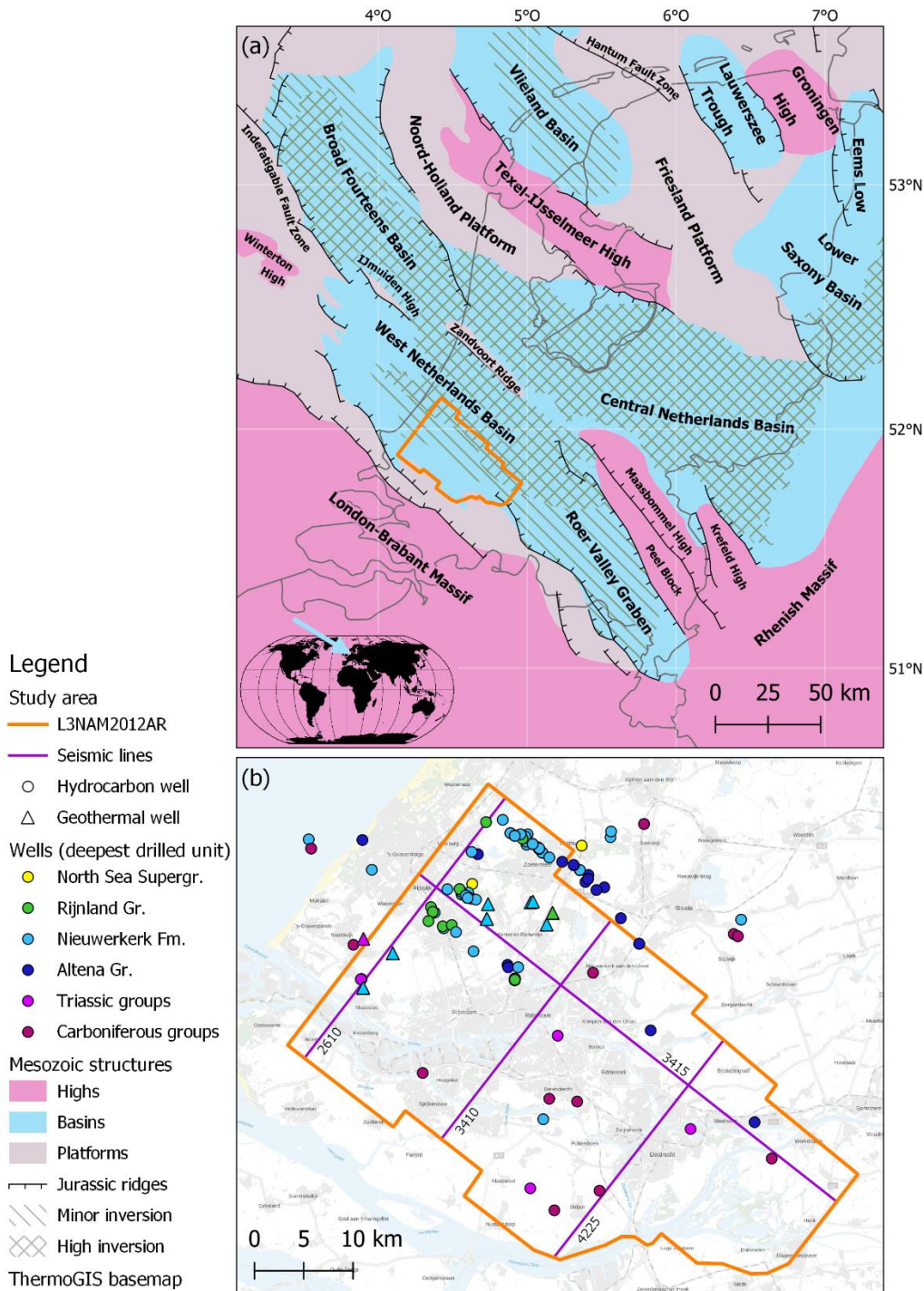
Figure 1: (a) Map of the Netherlands, showing the main structural elements during Jurassic times with the areas affected by the subsequent inversion marked. The seismic 3D cube is displayed in orange. This map was produced by combining the maps from Wong et al. (2007) & Kombrink et al. (2011). (b) Map of the study area, highlighted in orange, showing all used wells with their colours referring to the deepest encountered formation, and the seismic cross sections presented in figures 3, 4, 5 and 6.

70

4
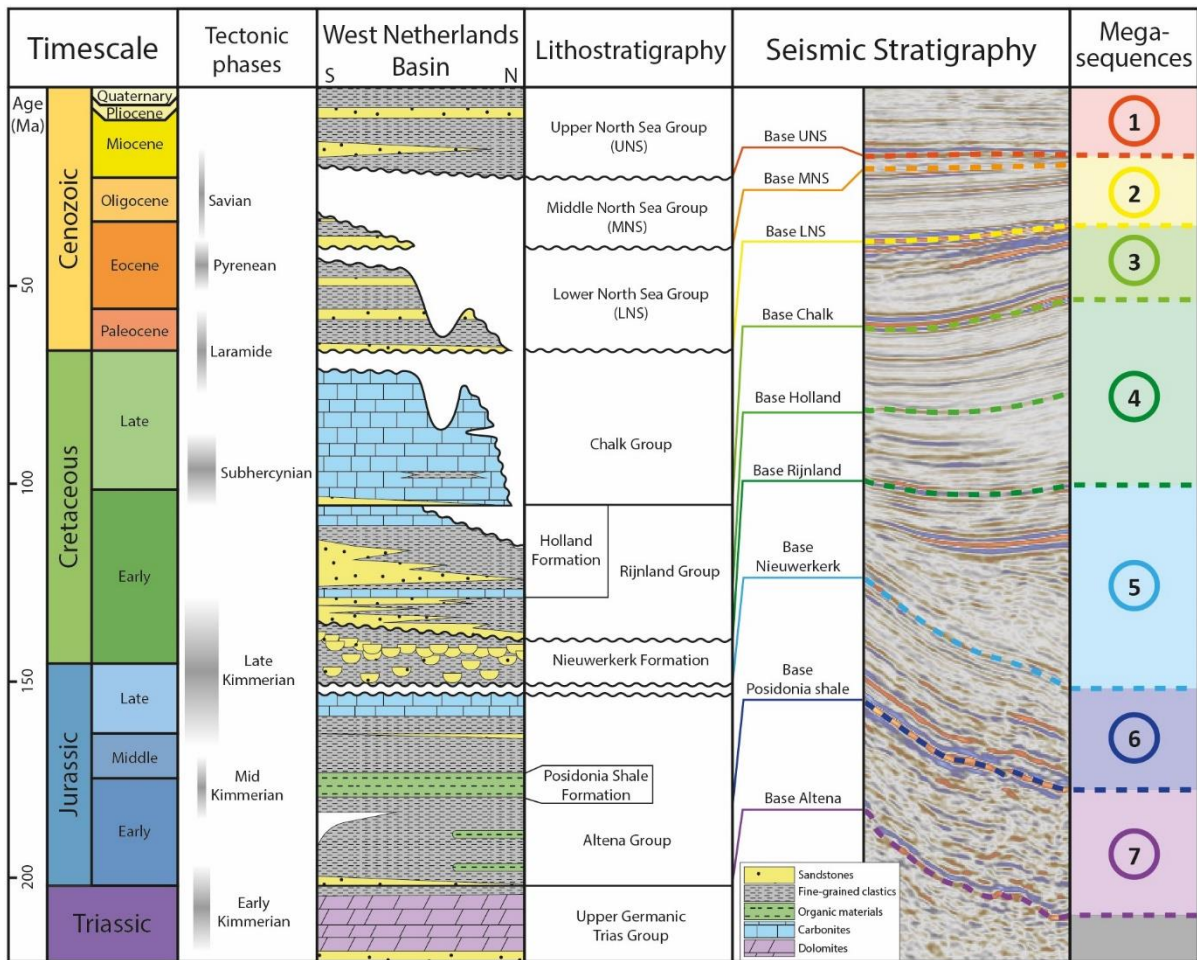
Figure 2: Lithostratigraphic chart, showing the timing of tectonic events, simplified stratigraphy of the studied section of the West Netherlands Basin, age of key horizons, and typical seismic stratigraphy for the study area. Stratigraphic column adapted from van Adrichem Boogaert & Kouwe (1993) & Jeremiah et al. (2010) and the timing of tectonic events adjusted from Wong et al. (2007) with the results from this study.

2 Geological framework

The West Netherlands Basin (WNB) is a NW-SE elongated basin in the western sector of the onshore Netherlands (Fig. 1a). The WNB developed above a former Paleozoic basin, forming part of the Southern Permian Basin, and partly retraces its structural trend (e.g. Ziegler, 1992; van Balen et al., 2000; Michon et al., 2003; Worum et al., 2005). Break-up of Pangea marks the onset of E-W oriented extension in NW Europe by the start of the Mesozoic (e.g. Ziegler, 1992). Regionally, the Triassic is characterised by uplift due to the Early Triassic Hardegsen tectonic phase (Geluk et al., 1996) and the Late Triassic Early Kimmerian tectonic phase (Geluk and Röhling, 1997). An Early Jurassic faulting phase is recognized in the area, causing

5

differential subsidence in the basin's various subunits (van Balen et al., 2000), followed by Middle Jurassic uplift, referred to as the Mid Kimmerian tectonic phase (Herngreen et al., 2003).

Despite the tectonic phases mentioned above, Late Permian to Middle Jurassic times are generally considered to be part of the pre-rift stage within the WNB (e.g. den Hartog Jager, 1996; Racero-Baena and Drake, 1996; van Balen et al., 2000; Vondrak et al., 2018; Willems et al., 2020). The WNB, characterised by horst and graben structures, is considered to be Late Jurassic (Kimmeridgian) to Late Cretaceous (Barremian), therefore this period is marked as the syn-rift phase (van Wijhe, 1987; den Hartog Jager, 1996; de Jager, 1996; Racero-Baena and Drake, 1996; Vondrak et al., 2018). In particular, the WNB developed during several discrete pulses of short duration from which the strongest phase occurred during the Late Jurassic, recognized as the Late Kimmerian tectonic phase (van Wijhe, 1987; de Jager, 1996; Racero-Baena and Drake, 1996; van Balen et al., 2000). The rifting resulted in the fragmentation of the WNB in several sub-basins, where local differential subsidence resulted in large thickness variations within the Late Jurassic basin infill. After the conclusion of the rifting phases by the Albian, the WNB entered a post-rift subsidence phase (van Wijhe, 1987), until basin inversion, spanning from the Late Cretaceous to the Miocene (e.g. Ziegler, 1992; de Jager, 2003; Worum and Michon, 2005; Deckers and van der Voet, 2018; Kley, 2018).

The Late Permian to Cenozoic sedimentary succession of the WNB, described in detail in van Adrichem Boogaert and Kouwe (1993) and TNO-GDN (2023), starts with the Late Permian Zechstein Group. The very few deep wells that have been drilled into the Zechstein Group have encountered carbonates and shales, but no evaporites. This group is overlain by the clastic Triassic Under-Germanian Group, which includes the Volpriehausen, Detfurth and Hardegsen formations. On top, the Middle to Late Triassic Upper-Germanian Group is made of mixed carbonates and (silici)clastics. Our seismic interpretation starts with the overlying Early to Middle Jurassic Altena Group (Fig. 2), which is primarily composed of shallow-marine clays, but also carbonates and sandstones. The Altena Group includes the Posidonia Shale Formation, which forms a key seismic reflector. In the study area, the overlying Late Jurassic-Early Cretaceous Schieland Group includes only the Nieuwerkerk Formation, which is one of the main targets for geothermal exploration in the WNB (see above). It is characterised by lateral thickness variations associated with extensional faulting, and includes sandstones and shales that are both vertically stacked and laterally interfingered. Above is positioned the Cretaceous Rijnland Group, which includes the Vlieland Subgroup and Holland Formation. The clastics of the Vlieland Subgroup were deposited in a transgressional setting that turned into a shallow to deep marine environment in which the carbonate and siliciclastic sediments of the Holland Formation were deposited. The Late Cretaceous carbonates of the Chalk Group were deposited in a shallow marine environment during the main inversion phase. The Cenozoic succession is known as the North Sea Supergroup, composed of the clastics of the Lower, Middle and Upper North Sea Groups (e.g., van Adrichem Boogaert and Kouwe, 1993; Duin et al., 2006).

3 Data and methods

This study uses the L3NAM2012AR seismic 3D depth cube and well data (Fig. 1b), which recently became publicly available on nlog.nl, along with technical information (including data and procedure for depth conversion) about the survey. The seismic

coverage has a surface area of roughly 1300 km^2, with 2678 diplines (2500-5178) and 1714 strikelines (2273-3987), penetrating to a depth of 6 km. The 3D cube was depth reprocessed and converted by Shell in 2011, using 59 wells for the depth conversion. We will use the depth converted version of this seismic cube, as the velocity cube is not publicly available. Additional wells are available, from which we have used a total of 94 inside and 31 close by the study area, with a maximum depth of 4 km, and the deepest drilled formation being the Carboniferous Limburg Group. The well database, together with the available formation tops helped the seismic interpretation. Yet, some of the used wells date from the start of hydrocarbon exploration in the basin in the 50's, and with the lithostratigraphic nomenclature changing over time, not all available formation tops are matching, wherefore the unmatching well tops were neglected.

Analysis and interpretation is done using Petrel 2020.3 software, following the well-established workflow for interpretation of seismic datasets in extensional settings (e.g. O'Sullivan et al., 2022), which involves a reconstruction of the seismic stratigraphy by integrating well data with the identification of different seismic facies, unconformities, and brightly marked reflective horizons. In detail, 9 horizons were interpreted for the whole 3D cube. Such a 3D interpretation has allowed us to identify the major faults of the basin and produce thickness maps of the syn-rift deposits, shedding light on the tectono-sedimentary evolution of the single sub-basins. For the horizon interpretation, seismic to well tie was achieved by using the available well tops provided by TNO on nlog.nl. For each horizon, a grid of 25 diplines x 25 strikelines was made using a guided approach (guided autotracking + seeded 3D tools of Petrel). A continuous checking of the geological consistency of the interpretation was carried out during the interpretation, by considering the seismic facies of the mapped horizons and the occurrence of regional unconformities, as illustrated in Figure 2.

In detail, the bases of the Cenozoic Upper, Middle and Lower North Sea Groups, the base of the upper Cretaceous Chalk Group, the bases of the lower Cretaceous Holland Formation and Rijnland Group, the base of the upper Jurassic Nieuwerkerk Formation, the Posidonia Shale Formation and the base of the Altena Group were mapped (Fig. 2). Those horizons were selected either for their easily recognizable seismic facies or for their structural appearance (e.g. unconformities). The results section will describe three diplines and one strikeline that are considered representative for all structures found in the seismic 3D cube (Figs. 3-6). Also, six thickness maps and a depth map will be discussed (Fig. 7). The thickness maps were produced in Petrel by computing the difference in elevation between the base of the overlying package and the base of the package itself. Although such a difference is not the actual thickness, given the horizons are characterised by very gentle dip (mostly less than 5°), it represents a reliable proxy. Exceptions are those areas of steeply dipping layers associated with tight folds. Also, the difference in elevation returns artefacts across faults, in which the top and bottom horizons are located in the hanging wall and footwall, respectively. Those two exceptions are recognisable in maps as narrow ribbons of anomalous thickness values, mostly overlapping the major faults.
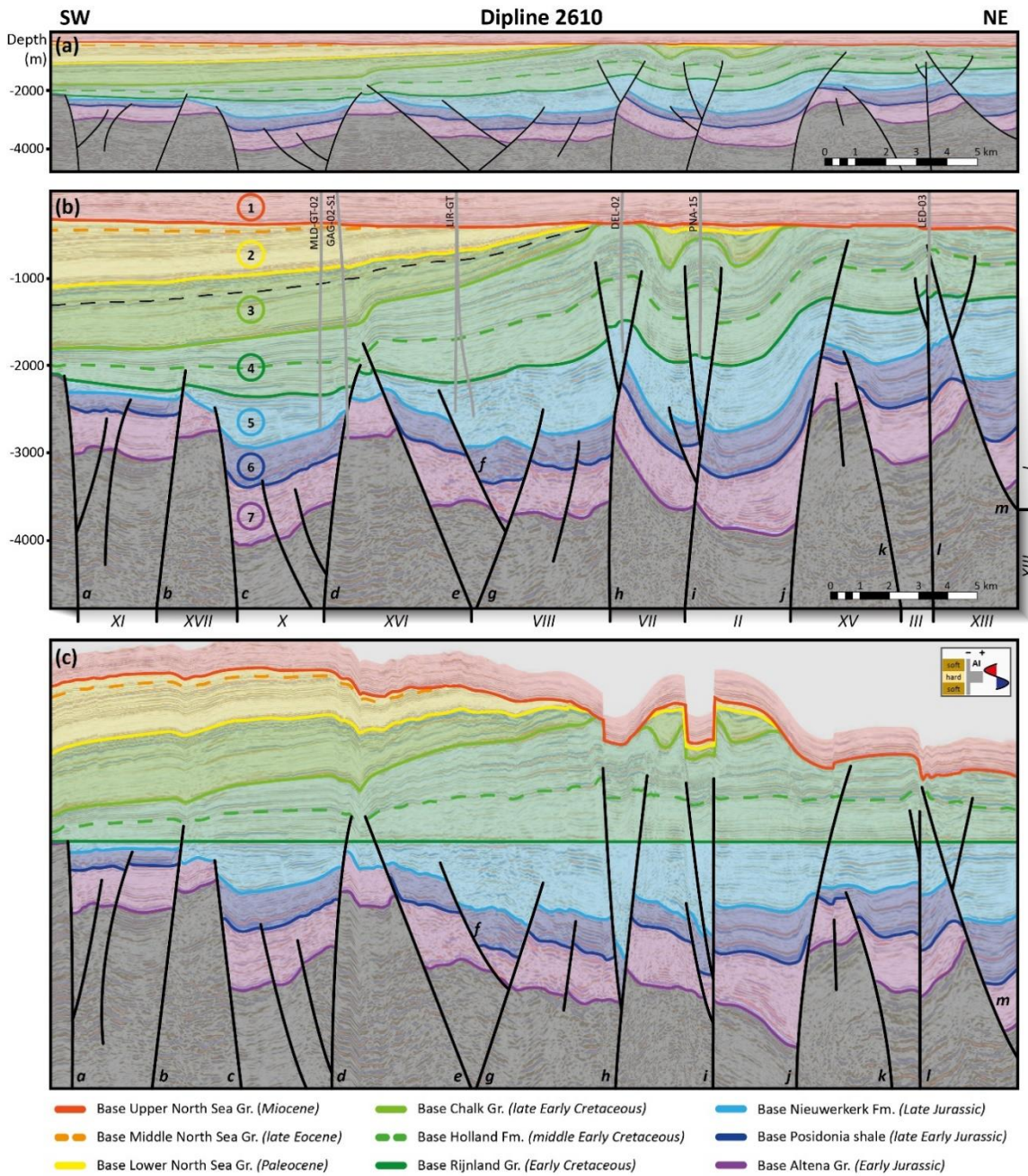
Figure 3: Dipline 2610 displayed with three different scales; (a): 1:1 scale, displayed with the interpreted horizons, megasequences and faults; (b): 1:3 scale, displayed with the interpreted horizons, megasequences and faults, together with projected wells and the unconformity within megasequence 3 (marked by the black dotted line). Below the section, the sub-basins and highs are numbered as in Figure 7 ((XI): Voorne Graben, (XVII): Hoek van Holland High, (X): Maasland Graben, (XVI): De Lier High, (VIII): Westland Graben, (VII): Rijswijk Graben, (II): Voorburg Graben, (XV): Zoetermeer High, (III): Zoetermeer Graben, (XIII): Moerkapelle High, (I): Waddinxveen Graben); (c): the 1:3 scaled section flattened for the base of the Rijnland Group, displayed with the interpreted horizons, megasequences and faults.

4 Results

4.1 Seismic sections

Here we present three SW-NE sections oriented perpendicular to the main trend of faults affecting the WNB, and one section oriented NW-SE (Fig. 1b). Up to the top of the Triassic, the stratigraphic succession can be divided into seven megasequences, here described from top to bottom. For each section, we present a 1:1 and 1:3 vertically exaggerated interpreted lines, along with a 1:3 vertically exaggerated one, flattened to the base of the Rijnland Group. The non-interpreted sections can be found in the Supplementary Materials.

4.1.1 Dipline 2610

Dipline 2610 (Fig. 3) is located on the NW edge of the study area (Fig. 1b). The section is crosscutting the Pijnacker (PNA-15) and Rijswijk (DEL-02) abandoned oil fields, and the Gaag (GAG-02-S1) and the De Lier (LIR-GT wells) producing gas fields. The Leidschendam (LED-03) abandoned gas field and two producing open loop geothermal energy projects (MLD-GT-02 & LIR-GT wells) are nearby.

Megasequence 1 is positioned between the top of the seismic cross-section and the base of the Upper North Sea Group. The package is characterised by sub-horizontal reflectors and an evident erosional surface at the bottom, forming an angular unconformity and toplap surface. Megasequence 2 is found beneath this erosional surface, towards the SW. This megasequence is eroded in the NE part of the section and contains the Middle and Lower North Sea Groups. To the SW, the package is slightly tilted, dipping a few degrees towards the SW. An unconformable contact divides megasequences 2 and 3. In detail, towards the SW, reflectors of megasequence 2 and 3 are parallel to each other, whereas in the Westland Graben (structure VIII, Fig. 3b), an erosional unconformity is dividing them (the unconformity is also found in the well PNA-15). Megasequence 3 is composed of the Chalk Group, which is thinning towards the NE. Around well PNA-15 we observe two growth synclines capped by the unconformity with the overlying megasequences 1 and 2. The upper part of this megasequence is locally divided from the central and lower ones by an unconformity (dashed black line, Fig. 3b). The apparent NE-ward thinning of this megasequence is mostly due to the erosional surface that marks the base of megasequence 1. The underlying megasequence 4 comprises the Rijnland Group. Oppositely to megasequences 2 and 3, this package is thinning towards the SW and it is affected by synclines and fault-cored anticlines, across which no remarkable thickness changes are observed, as illustrated in the flattened section (Fig. 3c). Despite some local anomalies (associated with the flattening procedure and the presence of faults) the flattened profile shows that megasequence 4 has a regional thinning, which does not change across the faults and folds. It is worth mentioning that none of the major faults seen in the section propagates across the upper portion of megasequence 4, leaving the youngest three megasequences un-faulted. Megasequence 5, which corresponds to the Nieuwerkerk Formation, is characterised by abrupt thickness changes across the numerous faults affecting the megasequence. Below, megasequence 6, composed of the upper part of the Altena Group and based by the Posidonia Shale Formation, is characterised by parallel

reflectors and thickness variations related to erosion atop structural highs. Finally, megasequence 7, comprising the lower part of the Altena Group, displays both parallel reflectors and a few growth geometries at fault-bounded sub-basins.

The seismic line crosses 12 major faults. Some of them display normal offsets, while others show normal offset in the lowermost tracts and reverse displacement in the upper portions, which is a diagnostic feature of fault inversion (Williams, 1989). All major faults affect the megasequences 5 to 7, whereas only those showing evidence of positive inversion propagate into megasequence 4. As previously mentioned, megasequences 1 to 3 are un-faulted. In detail, faults labelled *a* to *d*, define horst and graben structures. In the graben structures, megasequence 5 is characterised by half-grabens, whereas in the horst the thickness of megasequences 5 to 7 is strongly reduced. None of these faults show remarkable evidence of inversion and the lowermost part of megasequence 4 seals all of them. Faults *e* and *h* bound a pop-up structure resulting from the inversion of these two former normal faults and the uplift of the previous sub-basin depocenter. Faults *f* and *g*, which show no evidence of inversion, were part of the array of extensional faults within this depocenter. In detail, the inversion of the SW boundary fault *e* caused fault-propagation-folding registered by "contractional" growth strata in megasequence 3. Inversion of the NE boundary fault *h* was accompanied by the development of an antithetic fault, forming a second-order pop-up structure that is affecting megasequence 4. To the NE, fault *i* is SW-dipping and syn-sedimentary with respect to megasequence 5. Its inversion is accompanied by the development (or inversion) of two conjugate NE-dipping faults and produces another second-order pop-up structure, whose development is recorded by growth geometries in megasequence 3. Fault *j* displays evidence of positive inversion and, more importantly, bounds a half-graben (the Voorburg Graben, structure II, Fig. 3b) in which megasequence 7 displays clear evidence of growth-wedge geometry. The NE-dipping fault *k* is also bounding a semi-graben (the Zoetermeer Graben, structure III, Fig. 3b) in which both megasequence 5 and 7 are characterised by thickness variations. Accordingly, the fault has been active during the deposition of megasequences 5 and 7. It is worth mentioning that it has not been reactivated during inversion. Last, fault *l* is NE-dipping and has been active during deposition of megasequence 5. It is slightly inverted as suggested by the gentle anticline deforming megasequence 4. Apart from the clear evidence of reverse offset on normal faults, folding of reflectors both in the hanging- and footwalls of some faults (e.g. in the footwall of fault *l* or in the hanging wall of faults *e* and *k*), reveals possible buttressing effect (i.e. folding and second order faulting of the hanging wall and footwall without slip reversal along the master fault).

4.1.2 Dipline 3410

Dipline 3410 (Fig. 4) is located 16 km to the SE of dipline 2610 (Fig. 1b). The section crosses the Rotterdam and Oud-Beijerland Noord producing oil fields and the Pernis and Hekelingen producing gas fields. Close-by are the IJsselmonde (IJS-64-S2) and Berkel (BRK-07) abandoned oil fields.

Also here, megasequence 1 shows sub-horizontal reflectors based on an extensive erosional surface. Below, in the SW part of the section, megasequence 2 shows gently tilted parallel reflectors that become eroded towards the NE. Again, an unconformable contact separates megasequences 2 and 3, the latter showing substantial thinning towards the NE as well. Megasequence 3 displays low-amplitude synclinal and anticlinal structures, well evident at its base, capped by the

unconformably overlying megasequence 2. Similarly to the seismic line shown in Figure 3, also in this line we observe an unconformity between the uppermost part of the megasequence 3 and the central and lower part of it (black dashed line in Fig. 4b), such an unconformity appears to be gently folded. The underlying megasequence 4 shows parallel reflectors thinning towards the SW, as well evident in the flattened seismic profile (Fig. 4c), disrupted by faults. In the NE part of the section, the megasequence is partly eroded and directly toplapping onto megasequence 1. None of the major faults propagate across the top part of megasequence 4, which leaves the youngest three megasequences un-faulted. Below, megasequence 5 is affected by a number of faults and displays abrupt thickness changes. The thickness changes are even more clearly visible on the flattened section (despite all the limitations and biases of the flattening procedure), where the package shows at least four distinct asymmetric fault-bounded half-grabens. Also here, the underlying megasequence 6 is characterised by parallel reflectors and, contrasting to section 2610, megasequence 6 does not show significant thickness changes. The lowermost megasequence 7 displays both parallel layers, slight thickness changes and a fault-bounded half-graben at the NE part of the section.

Seven major faults are recognized in this seismic section, both normal and partly (in the lowermost tracts) inverted. Megasequences 5 to 7 are affected by all the faults, whereas only the faults showing positive inversion are propagating into megasequence 4, leaving megasequences 1 to 3 un-faulted. Part of the faults (*c*, *d*, *h*, *i* and *k*) from dipline 2610 extend in this section. In detail, faults *c* and *d* bound a structural high (the De Lier High, structure XVI, Fig. 4b) with small horst and graben structures. Here, megasequence 5 is absent and both structures and faults are capped by the uppermost part of megasequence 4. Fault *c* and the smaller faults within the bound structure show notable evidence of inversion. However, contrasting to section 2610, where fault *d* does not display clues of inversion, here inversion of the NE boundary of fault *d* resulted in the development of antithetic fault *n*. Together, the faults formed a set of small pop-up structures and a fault-propagation fold atop fault *n*, registered in megasequence 4. Faults *h* and *i* show a similar geometry, being SW-dipping and syn-sedimentary with respect to megasequence 5. Inversion of both faults is accompanied by the development of fault-propagation folds in megasequence 4. It ©s interesting to mention that both faults formed second-order pop-up structures in section 2610. In between faults *h* and *i*, fault *o* is recognized and together, these three faults bound two elegant semi-grabens (the Rijswijk and Pijnacker grabens, structures VII and IV, Fig. 4b) in which megasequence 5 shows clear growth geometries. Inversion of fault *o* caused the development of an antithetic fault, forming a second-order pop-up structure. Both the development of the fault-propagation folds and the second-order pop-up structure as result of the inversion of faults *d*, *h*, *o* and *i* recorded by growth geometries in megasequence 3. Last, also here, fault *k* is not inverted, but more importantly, it is bounding a semi-graben (the Zoetermeer Graben, structure III, Fig. 4b) in which both megasequence 5 and 7 are characterised by thickness variations. Like in section 2610, evidence for fault inversion is clear with folding of reflectors (e.g. in the hanging wall of fault *d* and footwall of fault *i*) revealing a buttressing effect upon inversion.
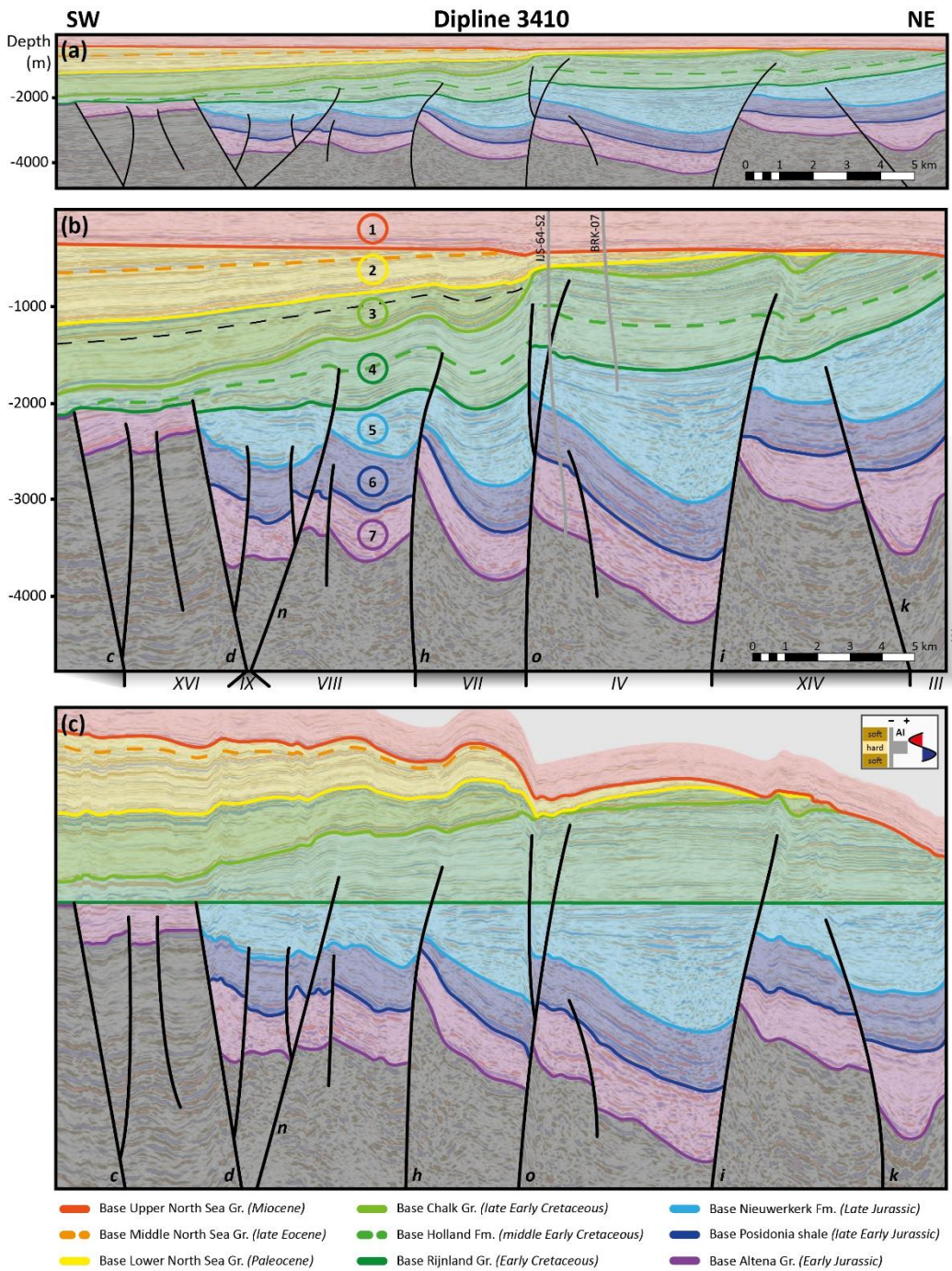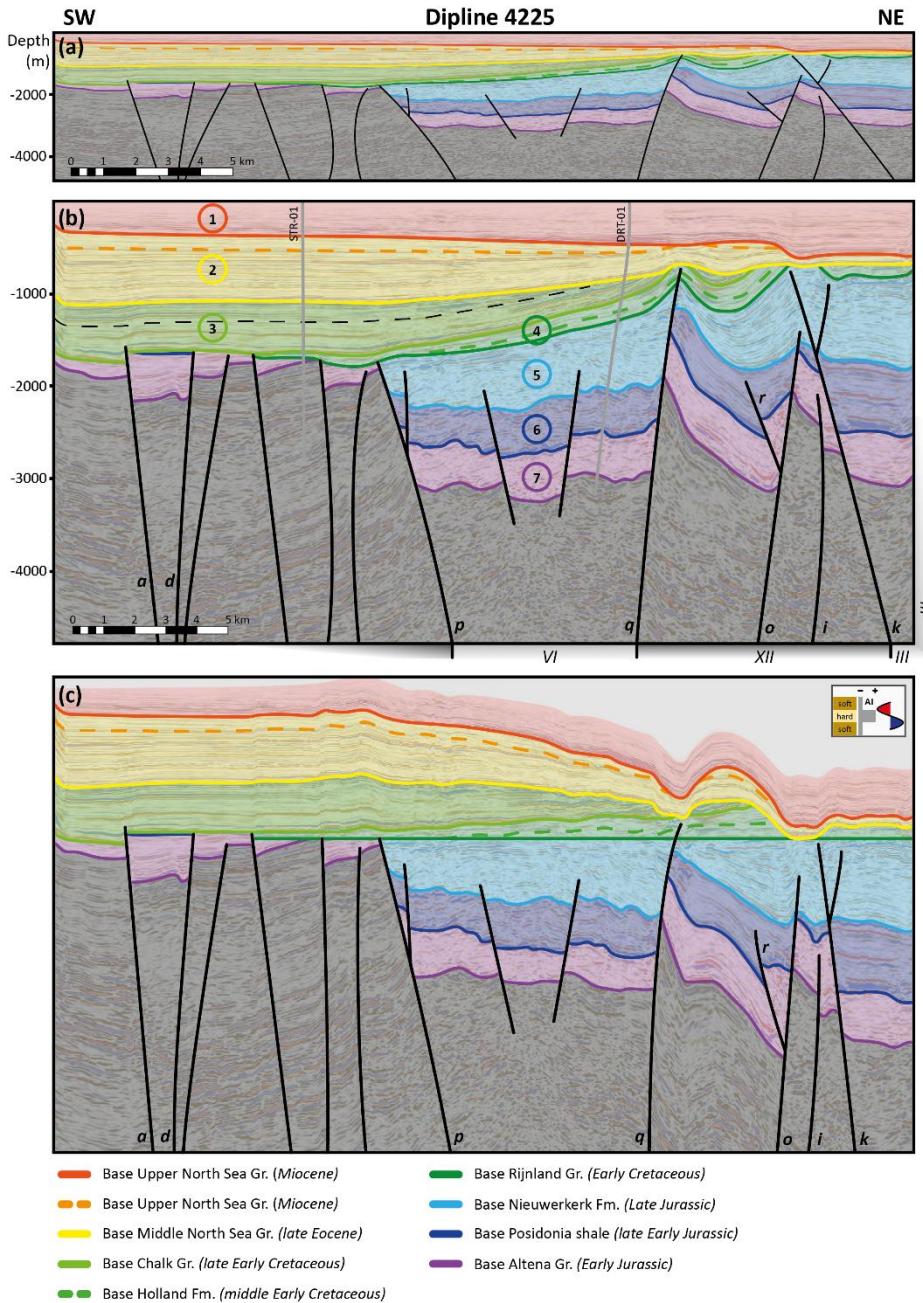
Figure 4: Dipline 3410 displayed with three different scales; (a): 1:1 scale, displayed with the interpreted horizons, megasequences and faults; (b): 1:3 scale, displayed with the interpreted horizons, megasequences and faults, together with projected wells and the unconformity within megasequence 3 (marked by the black dotted line). Below the section, the sub-basins and highs are numbered as in Figure 7 ((XVI): De Lier High, (IX): Spijkenisse Graben, (VIII): Westland Graben, (VII): Rijswijk Graben, (IV): Pijnacker Graben, (XIV): Lansingerland High, (III): Zoetermeer Graben); (c): the 1:3 scaled section flattened for the base of the Rijnland Group, displayed with the interpreted horizons, megasequences and faults.

12

SW Dipline 4225 **NE**

Legend:

- ▬ Base Upper North Sea Gr. *(Miocene)*
- ▬ ▬ Base Upper North Sea Gr. *(Miocene)*
- ▬ Base Middle North Sea Gr. *(late Eocene)*
- ▬ Base Chalk Gr. *(late Early Cretaceous)*
- ▬ ▬ Base Holland Fm. *(middle Early Cretaceous)*
- ▬ Base Rijnland Gr. *(Early Cretaceous)*
- ▬ Base Nieuwerkerk Fm. *(Late Jurassic)*
- ▬ Base Posidonia shale *(late Early Jurassic)*
- ▬ Base Altena Gr. *(Early Jurassic)*

Figure 5: Dipline 4225 displayed with three different scales; (a): 1:1 scale, displayed with the interpreted horizons, megasequences and faults; (b): 1:3 scale, displayed with the interpreted horizons, megasequences and faults, together with projected wells and the unconformity within megasequence 3 (marked by the black dotted line). Below the section, the sub-basins and highs are numbered as in Figure 7 ((VI): Dordrecht Graben, (XII): Ridderkerk Graben, (III): Zoetermeer Graben); (c): the 1:3 scaled section flattened for the base of the Rijnland Group, displayed with the interpreted horizons, megasequences and faults.

13

4.1.3 Dipline 4225

265   Dipline 4225 (Fig. 5) is located 16 km SE of dipline 3410 (Fig. 1b) and it does not crosscut any wells of an hydrocarbon field or geothermal energy projects. From the projected wells (Fig. 5b), STR-01 resulted in oil and gas shows, while well DRT-01 was dry.

In this line, megasequence 1 shows subhorizontal reflectors, floored by a major erosional surface. Below, megasequence 2 shows gently dipping reflectors, becoming eroded on top by the basal unconformity of megasequence 1 towards the NE. The

270   underlying megasequence 3 shows reflectors parallel to megasequence 2 towards the SW, while towards the NE, above the Dordrecht Graben and Ridderkerk Graben (structures VI and XII, Fig. 5b) an unconformity is separating these two megasequences. The intra-sequence unconformity that separates the uppermost part of megasequence 3 from the lower part, also observed in diplines 2610 and 3410, is observed here as well (black dashed line in Fig. 5b). In the SW, megasequence 3 is affected by faults. The underlying megasequence 4 is thinning towards the SW, being affected by a syncline and fault-cored

275   anticlines towards the NE. Towards the NE, megasequence 4 gets eroded by both megasequence 2 and 3. Except for fault *a*, none of the faults propagates across the top part of megasequence 4. Below, megasequence 5 is only present towards the NE portion of the section. Like in the previous diplines, megasequence 5 is affected by a number of faults and shows abrupt thickness changes, even better visible on the flattened section (Fig. 5c). In the Ridderkerk Graben (structure XII, Fig. 5b), megasequence 5 forms a fault-bounded half-graben. The underlying megasequence 6 is characterized by parallel reflectors,

280   only showing a thickness change in the NE part of the Ridderkerk Graben, related to erosion atop former structural highs. Lastly, megasequence 7 is characterized by both parallel layers and slight thickness changes.

Twelve major faults are recognized in this seismic section, from which eight will be described, comprising both normal and partly (in the lowermost tracts) inverted faults. Megasequences 5 to 7 are affected by all the faults, whereas only the faults showing positive inversion affect megasequence 4. Contrasting to diplines 2610 and 3410, megasequence 3 is affected by one

285   inverted fault, fault *a*. Above, megasequences 2 and 1 are not affected by faults. Part of the faults (*a*, *d*, *i*, *k*) from dipline 2610 and part of the faults (*d*, *i*, *k*, *o*) from dipline 3410 extend in this section. The SW-side of fault *p* represents the edge of the WNB, containing the four major faults that are not numbered, forming horst-and-graben structures (between faults *p* and *a*). Here, only megasequence 7 and a thin layer of megasequence 6 is present and the structures are capped by either megasequence 3 or 4. Faults *a* and *d* from the previous sections extent into this domain, from which fault *a* shows a positive inversion,

290   resulting in a small offset in megasequence 3. This is contrasting to section 2610, where fault *a* doesn't show inversion and is capped by megasequence 4. Faults *p* and *q* bound a graben (the Dordrecht graben, structure VI, Fig. 5b) that shows some internal normal faulting. Both fault *p* and *q* show positive inversion features in their top segments, evidenced by an antithetic fault in the upper part of fault *p* and the development of a fault-cored anticline in megasequence 4 atop fault *q*. Towards the NE, faults *q* and *k* bound a half-graben (the Ridderkerk Graben, structure XII, Fig. 5b). Below this semi-graben, a former

295   structural high can be found, bound by faults *o* and *k*. Similar to section 3410, inversion of fault *o* resulted in the development of an antithetic fault, here called fault *r*, but here only megasequences 6 and 7 are affected by this antithetic fault. Inside the

former structural high, fault *i* is normally faulting megasequence 7. This is contrasting to the previous sections, where fault *i* is expressed as a major fault with positive inversion in the upper segment. Towards the NE, like in section 3410, fault *k* bounds the Zoetermeer Graben (structure III, Fig. 5b). Contrasting to the previous sections where fault *k* does not show evidence of

300   inversion, here an antithetic fault formed in the upper segment as the result of reverse offset.
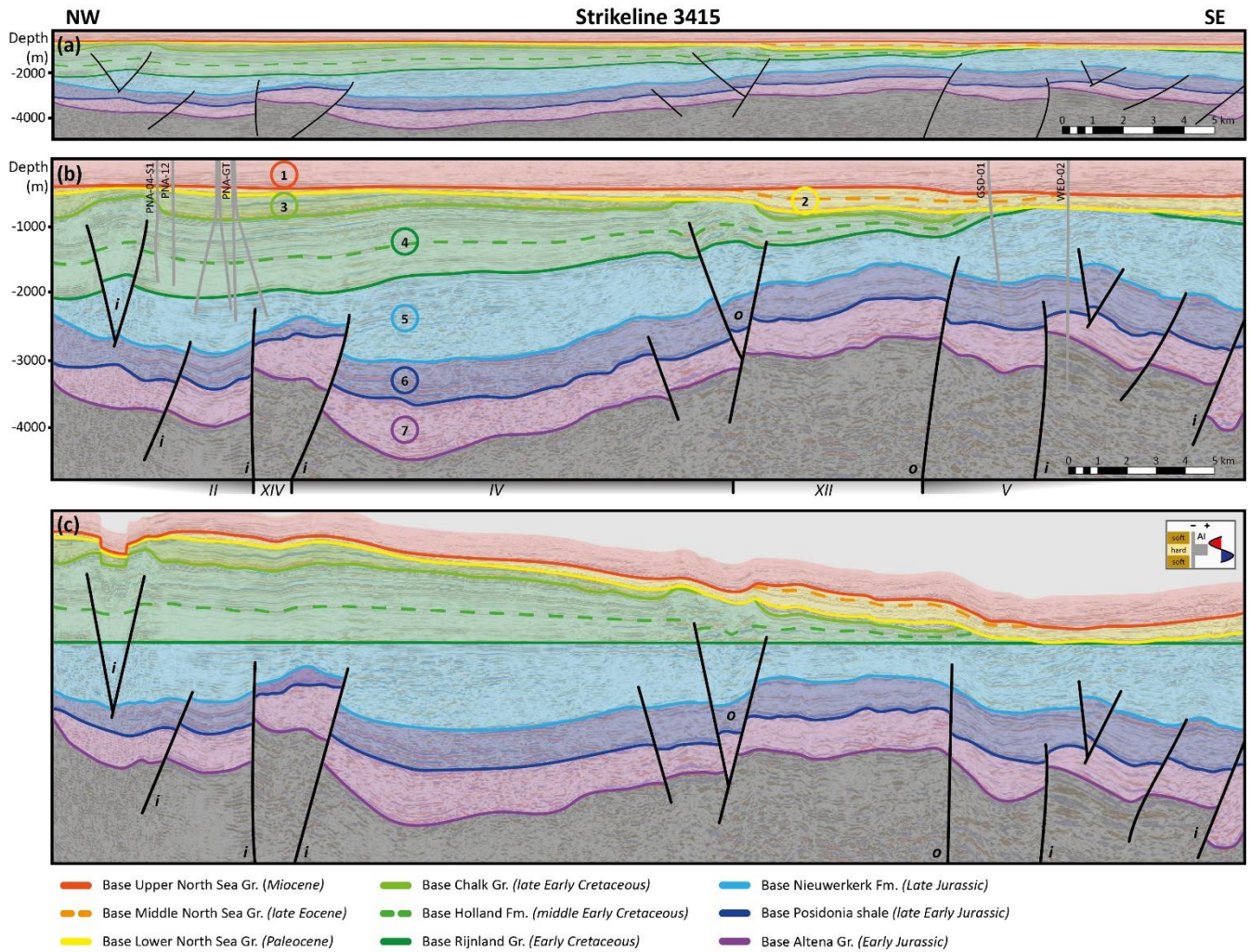
Figure 6: Strikeline 3415 displayed with three different scales; (a): 1:1 scale, displayed with the interpreted horizons, megasequences and faults; (b): 1:3 scale, displayed with the interpreted horizons, megasequences, faults and projected wells. The strikeline intersects fault i several times, wherefore the fault can be recognized multiple times. Below the section, the sub-basins and highs are numbered

305   **as in Figure 7 ((II): Voorburg Graben, (XIV): Lansingerland High, (IV): Pijnacker Graben, (XII): Ridderkerk Graben, (V): Biesbosch Graben); (c): the 1:3 scaled section flattened for the base of the Rijnland Group, displayed with the interpreted horizons, megasequences and faults.**

4.1.4 Strikeline 3415

Strikeline 3415 (Fig. 6) runs perpendicular to the previously described lines and crosses the NE part of the study area (see Fig.
1b), the Werkendam abandoned oil field (WED-02) and the undeveloped Werkendam-Diep gas field. Closeby is the GSD-01
well, the Pijnacker (PNA-04-S1 & PNA-12) abandoned oil field and a producing geothermal energy project (PNA-GT wells).
Megasequence 1 is characterised by subhorizontal reflectors and is bottomed by an erosional surface. Megasequence 2 is
characterised by thickness variation associated with uplift and erosion, whereas megasequence 3 displays growth geometries
with respect to faults i and o. Megasequence 2 toplaps megasequence 3, the latter disappearing towards the SE. The base of
megasequence 2 truncates open anticlines and synclines, with evident erosion of megasequences 3, 4 and 5. Megasequence 4
shows thinning towards the SE with parallel reflectors and no distinct thickness variations across short distances. Below,
megasequence 5 is characterised by thickness variations across short distances. No clear boundary faults can be identified in
this line for the growth-structures hosted in megasequence 4, evidencing that the major faults are oriented at low angle to this
seismic section. Also, within the package of megasequence 5, differing appearances of reflectors are observed, pointing
towards variations of seismic facies. Underlying megasequence 6 does not show remarkable thickness variations, whereas
lowermost megasequence 7 shows some slight changes in thickness.

As section 3415 is oriented at a low angle to the main faults, less intense deformation and thickness variations are observed.
Fault i is oriented parallel to section 3415 and, as it extends throughout the whole 3D cube, this fault crosses the section several
times. The fault bends along the section when going to the SE. Minor folding is observed in megasequence 4 atop these sections
of fault i, but no distinct inversion structures are present. The steep attitude of fault i suggests the occurrence of oblique
segments along the trace of this fault. Last, in the middle of the section, fault o bounds the Ridderkerk Graben (structure XII,
Fig. 6b), and showing a second-order pop-up structure related to fault o (section 3410) on the NW-boundary of this horst. All
faults, except the horst structures related to faults I and o, are capped by megasequence 4, whereas the faults of the horst
structures are capped by the top-part of the latter.
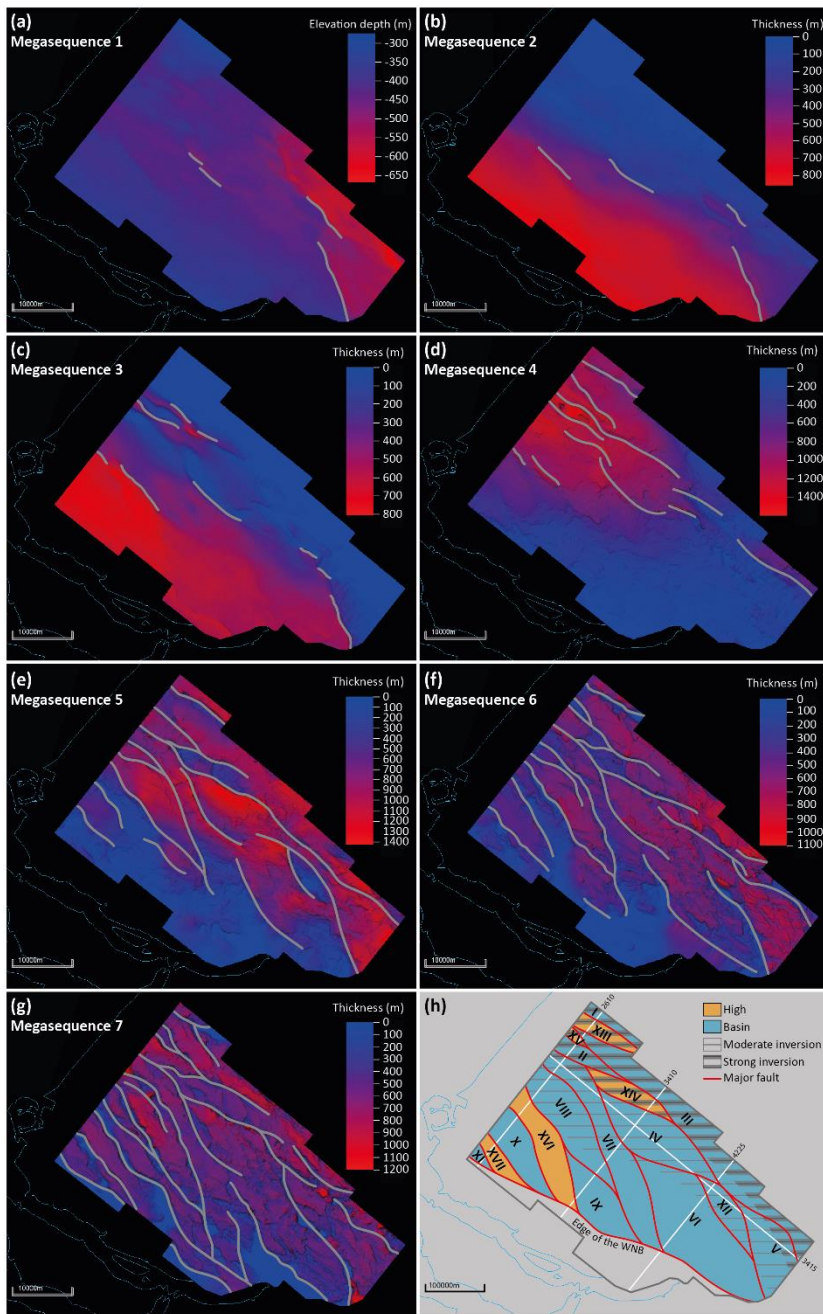
4.2 Thickness maps

Here, we present the thickness maps of megasequences 2 to 7 (Fig. 7b-g) and the depth map of the base of megasequence 1
(Fig. 7a). Megasequence 1 represents the youngest unit, therefore the depth map of its base is representative of its thickness.
Overall, megasequence 1 shows a constant thickness. Towards the E, an abrupt increase in depth is observed, related with the
only fault crosscutting this megasequence. Megasequence 2 shows a general thinning towards the NE, which is related to the
overlying erosional surface, but we also observe the occurrence of narrow NNW-SSE and NW-SE elongated areas with an
increased thickness. As seen in the seismic cross sections (Figs. 3 and 4), megasequence 3 was deposited during faults'
inversion.

This latter package displays an overall NE-ward thinning, related to the overlying erosional surface that is present at the base
of megasequence 1, with both NNW-SSE and (mostly) NW-SE elongated areas of increased/reduced thickness. Contrasting

340 to megasequence 3, megasequence 4 displays an overall thinning towards the S, with no localised areas of increased/decreased thickness. Megasequence 5 (the main geothermal target interval) is characterised by an overall thickness increase towards the NE. Areas of increased/reduced thickness are mostly lozenge-shaped with boundary faults being NW-SE and NNW-SSE oriented. Towards the S, megasequence 5 is almost absent due to erosion and/or non-deposition. Sub-basins filled by megasequence 5 are asymmetric, as evidenced by the sudden thickness change toward NE compared to a more gentle thickness

345 decrease towards the SW. Such an observation is suggestive of a first order architecture composed of half-graben structures bounded by SW-dipping master faults.

The interpretation of the thickness maps of megasequences 6 and 7 is less straightforward. These thickness maps show the effects of erosion during the deposition of megasequence 5, e.g., in the horst structure between faults *b* and *c* in section 2610 (Fig. 3). This effect is seen in the map as NNW-SSE oriented ribbons of reduced thickness, resembling horst structures. If we

Figure 7: (a): Depth map of megasequence 1, with present faults displayed in grey; (b-g): thickness maps of megasequences 2–7 with present faults displayed in grey; (h): Simplified map showing the structural elements formed as consequence of the first and second rifting episodes, together with a qualitative estimation of the degree of inversion. The seismic section displayed in figures 3-6 are displayed, together with the different highs and basins, which are numbered and named; (I): Waddinxveen Graben, (II): Voorburg Graben, (III): Zoetermeer Graben, (IV): Pijnacker Graben, (V): Biesbosch Graben, (VI): Dordrecht Graben, (VII): Rijswijk Graben, (VIII): Westland Graben, (IX): Spijkenisse Graben, (X): Maasland Graben, (XI): Voorne Graben, (XII): Ridderkerk Graben, (XIII): Moerkapelle High, (XIV): Lansingerland High, (XV): Zoetermeer High, (XVI): De Lier High, (XVII): Hoek van Holland High.

350

355

18

remove the effect of those ribbons from the thickness maps of megasequences 6 and 7, and we rely on the occurrence of growth

360   geometries (such as the growth wedge seen in megasequence 7 in the Voorburg Graben, structure II, close to fault *j*, Fig. 3b), we observe that the thickness distribution of megasequence 7 displays NW-SE elongated graben/semigraben, asymmetrically filled by growth strata wedging away from the master faults, and separated by horst structures. An outstanding example occurs in the northern corner of the map, where a 20 km long NW-SE elongated horst (the Lansingerland High, structure XIV, Fig. 7h) bound by two depocenters is observed. Megasequence 6 displays similar thickness variations, but none of the thickener

365   areas show growth wedge geometries, suggesting that thickness variations relate to later erosion rather than to syn-sedimentary creation of accommodation space.

5 Discussion

5.1 Tectonic evolution

The interpretation of the L3NAM2012AR seismic 3D cube has allowed us to subdivide the investigated sedimentary

370   succession into seven megasequences, corresponding to units spanning in age from Jurassic to Present times. Megasequences are delimited either by the occurrence of unconformities (base of megasequences 1, 2, 4 and 5), or by the transition from growth geometries (e.g. stratigraphic fanning/expansion-tapering, convergent reflectors) to parallel geometries. It is noted that intra-formational unconformities are present. However, in the framework of a sub-seismic structural reconstruction, only the main stratigraphical units are taken into account. Based on our observations, the evolution of the studied portion of the WNB

375   from the Jurassic onward can be assessed.

The first observed tectonic period can be dated to the Early Jurassic, which is the biostratigraphic age of the sedimentary rocks of megasequence 7. NW-SE elongated regions of decreased and increased thicknesses (Fig. 7g) are interpreted as related to Early to Middle Jurassic fault-bounded horst and graben structures, respectively. Growth geometries within this megasequence are observed, like the half-graben in the Voorburg Graben (structure II, associated with fault *j*, Fig. 3b). Coherently,

380   megasequence 7 is interpreted as a syn-rift sequence, with the thickness of syn-rift infill increasing towards the NE. Regionally, this rifting stage is synchronous with the final stage of the first rifting event that has shaped the North Sea Rift system (e.g. Fossen et al., 2021). This rifting event seems to coincide with the regionally recognized Early Kimmerian tectonics (Fig. 2) (Geluk and Röhling, 1997; Duin et al., 2006). The overlying megasequence 6 displays areas of slight thickness variation, but no growth geometries occur in it, therefore, it is to be considered post-rift. Overall, both megasequence 6 and 7 display a slight

385   NE-ward thickening, with the thickening direction being perpendicular to the direction of the main normal faults that were active during the Early Jurassic rifting stage. According to the widely recognised features in rift systems (e.g. Franke, 2013; Peron-Pinvidic et al., 2019), we interpret megasequence 6 as the post-rift passive infill of the accommodation space created synchronously with the deposition of megasequence 7. Since the timing of deposition of megasequence 6 corresponds to the inception of the thermal North Sea Rift Dome underneath the central North Sea (van Wijhe, 1987; Ziegler, 1992), an alternative

390   hypothesis could be that thinning of megasequence 6 is somehow related with this lithospheric-scale bulging process. Given

the centre of the dome was located far N (between NW Scotland and SE Norway) (Ziegler, 1992; Wong et al., 2007), N-ward thinning of megasequence 6 should be observed, which is not the case. Yet, it should be noted that later structural evolution could have overprinted subtle effects related to the North Sea Rift Dome. Still, the absence of N-ward thinning makes us discard the hypothesis of doming causing large impact on the depositional pattern of megasequence 6.

395 Deposition of the overlying megasequence 5 started in the Late Jurassic, during a second pulse of extensional faulting. The observed local unconformities within megasequence 5 suggest that faulting happened in several pulses. This stage is coeval with the second phase of rifting observed in the North Sea, further to the N (e.g. Færseth, 1996), which induced an enhancement crustal extension, known as the Late Kimmerian tectonics (van Wijhe, 1987; Ziegler, 1992; de Jager, 1996; Racero-Baena and Drake, 1996; van Balen et al., 2000). In the WNB, this extensional phase is simultaneous with igneous activity (Sissingh,
400 2004), a characteristic of continental rifting (e.g. Franke, 2013; Gouiza and Paton, 2019). We observe that the upper portion of megasequence 5 postdates all the normal faults (excluding those showing evidence of reverse reactivation). Several syn-depositional wedges (most of them being half-grabens) are observed in this megasequence, such as those associated with faults *h*, *o* and *i* in Figure 4. The various sub-basins active during this second extensional pulse are lozenge-shaped and they are bounded by NW-SE and NNW-SSE striking faults (Fig. 7e), the "zigzag" arrangement of faults being a typical feature when
405 pre-existing faults occur (e.g., Henstra et al., 2019). Many horst and graben structures active during this second rifting phase retrace structures developed during the first rifting stage, such as the ones seen in the NW part of the study area (e.g. the Westland Graben, structure VIII, Fig. 7h). The observation that during the first rifting stage the structures were NW-SE oriented, allowed us to infer that those NW-SE striking structures were reactivated during the second rifting phase. Accordingly, we deduce that the NNW-SSE striking normal faults formed during the second rifting phase. Such an inference
410 is coherent with natural examples and analogue models of multiphase rift systems, where it is commonly observed that oblique inherited structures can be reactivated synchronously with the formation of new faults oriented perpendicular to the stretching direction (e.g. McClay and White, 1995; Mart and Dauteuil, 2000; Henza et al., 2010; Brune et al., 2014; Naliboff and Buiter, 2015; Zwaan et al., 2016; Zwaan and Schreurs, 2017). An alternative hypothesis is that the lozenge-shaped structures are pull-apart basins or ridges associated with transtensive/transpressive faults. We discard this hypothesis for the studied area, as we
415 do not observe the diagnostic features of wrench tectonics, such as positive/negative flowers, branch faults, restraining/releasing bends, antithetic faults and/or strike-slip duplexes (e.g. Riedel, 1929; Wilcox et al., 1973; Harding, 1974; Aydin and Nur, 1982; Sanderson and Marchini, 1984; Woodcock and Fischer, 1986; Sylvester, 1988; among others) in the L3NAM2012AR seismic 3D dataset. Similarly to megasequences 7 and 6, megasequence 5 thickens towards the NE, suggesting that these megasequences form part of the same multiphase rift system.

420 After diminishing the rifting-related Jurassic crustal extensions (e.g. Ziegler, 1992), the WNB entered a post-rift phase by the Early Cretaceous (van Wijhe, 1987), during which megasequence 4 deposited. None of the observed extensional faults were active at that time. Post-rift infill of the WNB is well represented by megasequence 4 on the flattened displays of sections 2610 and 3410 (Figs. 3b & 4b) and on the thickness map, showing a NW-SE elongated, 20 to 40 km wide, post-rift basin (Fig. 7d).

Such a broad basin does not overlap the syn-rift grabens and, therefore, it likely relates to large-scale sagging rather than to
425   the simple passive infill of the previously developed half-grabens.

On top of the post-rift megasequence 4, the Lower Cretaceous megasequence 3 was deposited during a shortening stage. Positively inverted normal faults with associated growth geometries and buttressing-related structures are observed in this megasequence (e.g. associated with faults *e* and *i* in Fig. 3 and fault *a* in Fig. 5). This Late Cretaceous period of inversion likely corresponds to the Late Cretaceous Subhercynian inversion phase (Fig. 2) (e.g. Ziegler, 1992; van Wijhe, 1987; de Jager
430   2003, Worum and Michon, 2005), caused by the convergence between Africa and Europa (Kley and Voigt, 2008). During this stage, both faults of the NW-SE and NNW-SSE systems have been inverted or deformed during buttressing. Yet, we were not able to individuate newly formed reverse faults, which are needed to constrain the shortening direction. While the NE-section of the WNB got inverted and uplifted, its SW-flank became subject to subsidence and developed into a marginal basin, referred to as the Voorne Trough (Deckers, 2015) and well-illustrated by the SW-ward thickness increase of megasequence 3 (Fig. 7c).
435   The upper portion of megasequence 3 could already include a post-inversion succession. In fact, a local unconformity divides the upper from the central and lower portions of this megasequence, as illustrated in figures 3, 4 and 5. This is consistent with regional constraints, indicating that due to a decrease in convergence rate between Africa and Europa (Rosenbaum et al., 2002), the Subhercynian inversion ceased after the Campanian (de Jager, 2003), whereafter deposition of the chalk of megasequence 3 continued for the entire Late Cretaceous (van Balen et al., 2000; van der Voet et al., 2019).

440   Megasequence 2 is separated from the underlying megasequence 3 by a regional unconformity. No growth wedge geometries are observed in this megasequence, suggesting that the gentle folding of its base is associated with compaction of the underlying sediments and/or the passive infill/draping of a paleo-topography. Both syn-inversion megasequence 3 and post-inversion megasequence 2 thin out toward the NE, indicating that uplift of the NE sector of the study area started during faults' inversion but continued during the deposition of megasequence 2, as also evidenced by the SW-tilting of the erosional
445   unconformity separating the two megasequences. The erosional unconformity at the base of megasequence 2 likely corresponds to the timing of the Laramide uplift that peaked during the Middle Paleocene (Deckers, 2015), which may be related to a significant drop in global sea-level (Haq et al., 1987), along with a contribution from dynamic topography associated with mantle flow (Kley, 2018; Voigt et al., 2021). The Laramide tectonic phase is believed to have caused basin uplift in the area of the WNB (Deckers and van der Voet, 2018; Kley, 2018). The erosional unconformity at the top of
450   megasequence 2, instead, reflects the broad basin uplift (de Jager, 2003), likely initiated by the Alpine Orogeny (Worum and Michon, 2005). Lastly, the depth map of the base of megasequence 1 displays two large plateaus, separated by an ENE-dipping fault formed during the second extensional phase and reactivated during these times.

5.2 Implications for geothermal systems

The WNB harbours well developed geothermal reservoir rocks and is covered by a good data-collection, inherited from former
455   hydrocarbon exploration. Presently, the most exploited geothermal reservoir units are the Late Jurassic Nieuwerkerk Formation (megasequence 5; second syn-rift) and, subordinately, the Cretaceous sandstones (megasequence 4, post-rift and pre-

inversion). An additional reservoir is represented by the Triassic sandstones, which occur at deeper structural levels, and have not been mapped in this work. Yet, although the observed first rift is Early Jurassic in age, its rifting architecture might be applicable to the Triassic reservoir as well. Rift initiation already happened during the Triassic (e.g. Ziegler, 1992; van Wijhe, 1987), wherefore the Early Jurassic rift possibly is a remnant from Triassic extensional tectonics. Although the Triassic sandstones are known for having a reduced reservoir quality (Boersma et al., 2020), underneath the Zoetermeer High (structure XV in figs. 3b and 7h) the reservoir quality might be better. Here, the structural high seems to have been relatively stable throughout the evolution of the basin, as evidenced by fault *k* showing no signs of reactivation during inversion (Fig. 3). Therefore, the Triassic reservoir might be less fractured with shallower burial conditions than in the surrounding grabens.
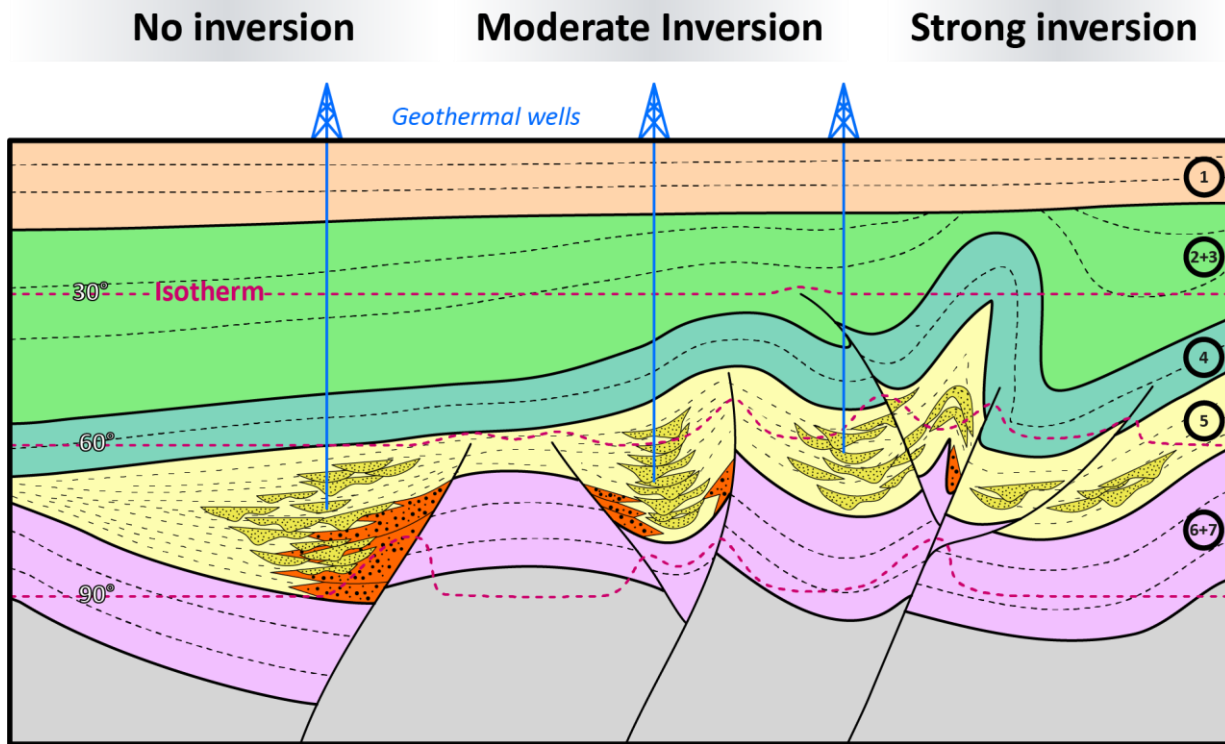
Figure 8: Simplified figure, showing the geothermal play of a fluvial-deltaic reservoir in an inverted rift basin. The expected best spots for geothermal exploration are the central portions of the growth synclines, where the fluvial sands (yellow dotted material) are present, geothermal gradients are highest and interference from foot-wall erosion (orange dotted material) is minor. The isotherms are based on a geotherm of 31°C km^{-1} (Bonté et al., 2012). The sketched layers correspond to the interpreted megasequences of this study, indicated in the circles on the right side.

Among the two Jurassic-Cretaceous reservoirs, the Nieuwerkerk Formation is the most promising, facilitating a deeper reservoir (spanning in depth from 0.5 km to 3 km) and, given the geothermal gradient of the area (Fig. 8, 31°C km^{-1}; Bonté et al., 2012), likely offering temperatures up to 90°C, which is perfect for low enthalpy geothermal systems. Instead, temperatures for the Cretaceous sandstones probably do not exceed 60°C. The Nieuwerkerk Formation was deposited during the second rifting event in the Late Jurassic (megasequence 5) and the multi-phase extensional setting led to the development of a compartmentalised reservoir, made up of lozenge shaped sub-basins. Given the fluvial nature of the Nieuwerkerk Formation

(e.g. Willems et al., 2017c; Vondrak et al., 2018; Willems et al., 2020), the lateral and vertical compartmentalization of sands and shales is a characteristic that must be taken into account in the reservoir's geothermal exploration. In rift systems involving continental to coastal clastic syn-tectonic sedimentation, it is well known that the more coarse grained facies are located close to the faults and along the axis of grabens and half-grabens (e.g., Gawthorpe and Leeder, 2000). In agreement, we expect the fluvial channels and other coarse grained sediments to be located in the core of half-grabens or in their inner limb (i.e. the limb close to the master fault). Furthermore, close to the master fault, foot-wall erosion and related hanging-wall degradation complexes drive the development of a wide spectrum of heterogeneous sedimentary facies, possibly interfingering with the targeted reservoir rock. Contrasting to petroleum systems, in which structural highs are the preferential target for hydrocarbon exploration (hydrocarbons are lighter than water), half-grabens are the most suitable sites for geothermal exploration. Indeed, half-grabens are found at deeper levels, thus ensuring higher temperatures with respect to limbs and structural highs. Combining all that is stated above allows us to individuate the core of half-grabens, i.e. syn-tectonic intervals in the core of half-grabens, as preferential sites for geothermal exploration. Here, the chances of finding hot and thick fluvial sand packages with a higher nett to gross ratio, are increased.

Such a simple template is modified during faults' reactivation and buttressing associated with the inversion stage. Such an inversion can produce (1) the uplift of the former structural-stratigraphic reservoirs, i.e. the half-grabens, with the consequent decrease of water temperatures and, eventually, (2) fracturing of reservoirs by second order faults and brecciation and breaching of the reservoir when the amount of inversion increases (e.g. Tari et al., 2020). All the above discussed features are schematically illustrated in Figure 8, where normal faults, positively inverted normal faults, half-grabens, geotherms, and sweet spots are outlined.

Given the template illustrated in Figure 8 and assuming that the most suitable areas for geothermal exploration are the central portions of the half-grabens. Synclinal traps in half-grabens associated with strongly inverted faults are more likely to be breached by faults developed during inversion tectonics.

The effects of secondary fracturing due to inversion tectonics can be beneficial in terms of permeability. Instead, the consequences of breaching a geothermal reservoir due to inversion tectonics is less clear. In hydrocarbon reservoirs, indeed, breaching of the anticlinal traps has a clear negative effect (i.e. leakage of the hydrocarbons), while the consequences of breaching synclinal traps in geothermal systems are not yet fully understood. In order to de-risk geothermal exploitation, we therefore advise to choose half-grabens associated with either non-inverted or moderately inverted normal faults. By combining these findings, we can identify areas of interest for geothermal exploitation. Examples of such areas are the central portions of the Pijnacker, Rijswijk and Westland grabens (structures IV, VII and VIII, figs. 4, 7e and 7h). Here, the grabens contain a thick (1 to 1,4 km in thickness) package of Nieuwerkerk Formation, while displaying no to moderate inversion. The deepest portions of these grabens are located away from the master fault, preventing interference by material originating from foot-wall erosion. The centres of these grabens are located at depths roughly between 2 and 3 km, giving the present sand bodies expected temperatures between 60°C and 90°C (based on a geotherm of 31°C km^{-1}; Bonté et al., 2012). In such areas, additional work

510   is required to assess the fluvial reservoir architecture (Willems et al., 2017a) in more detail and properly locate injection and recovery wells (i.e. geothermal doublets) within coarse grained sediments.

6 Conclusion

A renewed seismic interpretation of the recently released L3NAM2012AR seismic 3D dataset, allowed a detailed study of the sub-seismic structural geology of the WNB, which helps better understand the regional sedimentary aquifer architecture. The
515   fault activation and reactivation, together with the development of its syn-rift infill were re-assessed. From Jurassic times onwards, seven megasequences were documented: (1) a first NE-SW oriented rifting phase during the Early Jurassic; (2) a post-rift phase during the Middle Jurassic; (3): a second WSW-ENE oriented rifting phase during the Late Jurassic, partly controlled by the Early Jurassic rifting phase; (4): an Early Cretaceous post-rift sag phase; (5): faults' inversion during the Late Cretaceous; (6): broad basin uplift during the Paleocene to Oligocene; (7): a minor reactivation event during the Miocene.
520   Multi-phase rifting during the Jurassic led to compartmentalization of the second syn-rift infill, which is the main geothermal target in the WNB; the Late Jurassic fluvial-deltaic Nieuwerkerk Formation. We expect its channel sands to be present in the deepest, central portions of the half-grabens, where the highest temperatures are expected. Here, interference by foot-wall erosion and residue hydrocarbons is expected to be minor. The Cretaceous inversion needs to be taken into account, as an increasing amount of inversion can form risks for geothermal exploration, as it could have caused breaching of the reservoir
525   and uplift of the targeted half-grabens, hence lowering the temperature. Therefore, only non to moderately inverted areas should be considered for geothermal exploration.

Hence, we conclude that for a geothermal play in a multi-phase rift setting with subsequent basin inversion and a fluvial-deltaic syn-rift reservoir rock, the best spots for geothermal exploration can be found in the central portions of non to moderately inverted half-grabens.

Supplementary materials

The supplementary materials; a list of used wells, links to the public datasets and files with the uninterpreted seismic lines can be found with this article.

Author contribution

AW, corresponding author, conceptualisation, data acquisition and processing, seismic interpretation, figures and manuscript
535   drafting/editing; KO, interpretation assistance, figures and manuscript drafting/editing; FV, data acquisition, manuscript drafting/editing; CL, data acquisition, interpretation assistance, manuscript drafting/editing; GB, manuscript drafting/editing;

JA, manuscript drafting/editing; ST, conceptualisation, data processing, interpretation assistance, figures and manuscript drafting/editing.

Competing interests

Acknowledgments

References

van Adrichem Boogaert, H. A. and Kouwe, W. P. F.: Stratigraphic nomenclature of the Netherlands, revision and update by
550 RGD and NOGEPA, 1993.

Aydin, A. and Nur, A.: Evolution of pull-apart basins and their scale independence, Tectonics, 1, 91–105, https://doi.org/10.1029/TC001i001p00091, 1982.

555 van Balen, R. T., van Bergen, F., de Leeuw, C., Pagnier, H., Simmelink, H., van Wees, J. D., and Verweij, J. M.: Modelling the hydrocarbon generation and migration in the West Netherlands Basin, the Netherlands, Netherlands Journal of Geosciences - Geologie en Mijnbouw, 79, 29–44, https://doi.org/10.1017/S0016774600021557, 2000.

Boersma, Q. D., Bruna, P. O., de Hoop, S., Vinci, F., Moradi Tehrani, A., and Bertotti, G.: The impact of natural fractures on
560 heat extraction from tight Triassic sandstones in the West Netherlands Basin: a case study combining well, seismic and numerical data, Netherlands Journal of Geosciences, 100, e6, https://doi.org/10.1017/njg.2020.21, 2021.

Bonté, D., van Wees, J. D., and Verweij, J. M.: Subsurface temperature of the onshore Netherlands: new temperature dataset and modelling, Netherlands Journal of Geosciences - Geologie en Mijnbouw, 91, 491–515, https://doi.org/10.1017/S0016774600000354, 2012.

Brune, S., Heine, C., Pérez-Gussinyé, M., and Sobolev, S. V.: Rift migration explains continental margin asymmetry and crustal hyper-extension, Nat Commun, 5, 4014, https://doi.org/10.1038/ncomms5014, 2014.

Carapezza, M. L., Chiappini, M., Nicolosi, I., Pizzino, L., Ranaldi, M., Tarchini, L., de Simone, G., Ricchetti, N., and Barberi, F.: Assessment of a low-enthalpy geothermal resource and evaluation of the natural CO_2 output in the Tor di Quinto area (Rome city, Italy), Geothermics, 99, 102298, https://doi.org/10.1016/j.geothermics.2021.102298, 2022.

Crooijmans, R. A., Willems, C. J. L., Nick, H. M., and Bruhn, D. F.: The influence of facies heterogeneity on the doublet performance in low-enthalpy geothermal sedimentary reservoirs, Geothermics, 64, 209–219, https://doi.org/10.1016/j.geothermics.2016.06.004, 2016.

Deckers, J.: The Paleocene stratigraphic records in the Central Netherlands and close surrounding basins: Highlighting the different responses to a late Danian change in stress regime within the Central European Basin System, Tectonophysics, 659, 102–108, https://doi.org/10.1016/j.tecto.2015.07.031, 2015.

Deckers, J. and van der Voet, E.: A review on the structural styles of deformation during Late Cretaceous and Paleocene tectonic phases in the southern North Sea area, J Geodyn, 115, 1–9, https://doi.org/10.1016/j.jog.2018.01.005, 2018.

DeVault, B. and Jeremiah, J.: Tectonostratigraphy of the Nieuwerkerk Formation (Delfland subgroup), West Netherlands Basin, AAPG bulletin, 86, 1679-1707, https://doi.org/10.1306/61EEDD50-173E-11D7-8645000102C1865D, 2002.

Duin, E. J. T., Doornenbal, J. C., Rijkers, R. H. B., Verbeek, J. W., and Wong, Th. E.: Subsurface structure of the Netherlands - results of recent onshore and offshore mapping, Netherlands Journal of Geosciences - Geologie en Mijnbouw, 85, 245–276, https://doi.org/10.1017/S0016774600023064, 2006.

Færseth, R. B.: Interaction of Permo-Triassic and Jurassic extensional fault-blocks during the development of the northern North Sea, J Geol Soc London, 153, 931–944, https://doi.org/10.1144/gsjgs.153.6.0931, 1996.

595 Fossen, H., Ksienzyk, A. K., Rotevatn, A., Bauck, M. S., and Wemmer, K.: From widespread faulting to localised rifting: Evidence from K-Ar fault gouge dates from the Norwegian North Sea rift shoulder, Basin Research, 33, 1934–1953, https://doi.org/10.1111/bre.12541, 2021.

Franke, D.: Rifting, lithosphere breakup and volcanism: Comparison of magma-poor and volcanic rifted margins, Mar Pet 600 Geol, 43, 63–87, https://doi.org/10.1016/j.marpetgeo.2012.11.003, 2013.

Gawthorpe, R. L. and Leeder, M. R.: Tectono-sedimentary evolution of active extensional basins, Basin Research, 12, 195–218, https://doi.org/10.1111/j.1365-2117.2000.00121.x, 2000.

605 Geluk, M. C. and Röhling, H. G.: High-resolution sequence stratigraphy of the Lower Triassic Buntsandstein in the Netherlands and Northwestern Germany, Geologie en Mijnbouw (Geology and Mining), 76, 227–246, https://doi.org/10.1023/A:1003062521373, 1997.

Geluk, M. C., Plomp, A., and van Doorn, T. H. M.: Development of the Permo-Triassic succession in the basin fringe area, 610 southern Netherlands, in: Geology of Gas and Oil under the Netherlands, Springer Netherlands, Dordrecht, 57–78, https://doi.org/10.1007/978-94-009-0121-6_7, 1996.

Geothermie Nederland: Locaties op de kaart, https://geothermie.nl/geothermie/locaties-op-kaart/, last access: 25 May 2023.

615 Gouiza, M. and Paton, D. A.: The Role of Inherited Lithospheric Heterogeneities in Defining the Crustal Architecture of Rifted Margins and the Magmatic Budget During Continental Breakup, Geochemistry, Geophysics, Geosystems, 20, 1836–1853, https://doi.org/10.1029/2018GC007808, 2019.

Harding, T. P.: Petroleum Traps Associated with Wrench Faults, Am Assoc Pet Geol Bull, 58, 620 https://doi.org/10.1306/83D91669-16C7-11D7-8645000102C1865D, 1974.

den Hartog Jager, D. G.: Fluviomarine sequences in the Lower Cretaceous of the West Netherlands Basin: correlation and seismic expression, in: Geology of Gas and Oil under the Netherlands, Springer Netherlands, Dordrecht, 229–241, https://doi.org/10.1007/978-94-009-0121-6_19, 1996.
625
Haq, B. U., Hardenbol, J., and Vail, P. R.: Chronology of fluctuating sea levels since the Triassic, Science, 235, 1156-1167, https://doi.org/10.1126/science.235.4793.1156, 1987.

Henstra, G. A., Berg Kristensen, T., Rotevatn, A., and Gawthorpe, R. L.: How do pre-existing normal faults influence rift geometry? A comparison of adjacent basins with contrasting underlying structure on the Lofoten Margin, Norway, Basin Research, 31, 1083–1097, https://doi.org/10.1111/bre.12358, 2019.

Henza, A. A., Withjack, M. O., and Schlische, R. W.: Normal-fault development during two phases of non-coaxial extension: An experimental study, J Struct Geol, 32, 1656–1667, https://doi.org/10.1016/j.jsg.2009.07.007, 2010.

Herngreen, G. F. W., Kouwe, W. F. P., and Wong, T. E.: The Jurassic of the Netherlands, Geological Survey of Denmark and Greenland Bulletin, 1, 217–230, https://doi.org/10.34194/geusb.v1.4652, 2003.

de Jager, J., Doyle, M. A., Grantham, P. J., and Mabillard, J. E.: Hydrocarbon habitat of the West Netherlands Basin, in: Geology of Gas and Oil under the Netherlands, Springer Netherlands, Dordrecht, 191–209, https://doi.org/10.1007/978-94-009-0121-6_17, 1996.

de Jager, J.: Inverted basins in the Netherlands, similarities and differences, Netherlands Journal of Geosciences - Geologie en Mijnbouw, 82, 339–349, https://doi.org/10.1017/S0016774600020175, 2003.

Jeremiah, J. M., Duxbury, S., and Rawson, P.: Lower Cretaceous of the southern North Sea Basins: reservoir distribution within a sequence stratigraphic framework, Netherlands Journal of Geosciences - Geologie en Mijnbouw, 89, 203–237, https://doi.org/10.1017/S0016774600000706, 2010.

Kley, J.: Timing and spatial patterns of Cretaceous and Cenozoic inversion in the Southern Permian Basin, Geological Society, London, Special Publications, 469, 19–31, https://doi.org/10.1144/SP469.12, 2018.

Kley, J. and Voigt, T.: Late Cretaceous intraplate thrusting in central Europe: Effect of Africa-Iberia-Europe convergence, not Alpine collision, Geology, 36, 839-842, https://doi.org/10.1130/G24930A.1, 2008.

Kramers, L., van Wees, J. D., Pluymaekers, M. P. D., Kronimus, A., and Boxem, T.: Direct heat resource assessment and subsurface information systems for geothermal aquifers; the Dutch perspective, Netherlands Journal of Geosciences - Geologie en Mijnbouw, 91, 637–649, https://doi.org/10.1017/S0016774600000421, 2012.

Kombrink, H., Doornenbal, J. C., Duin, E. J. T., den Dulk, M., ten Veen, J. H., and Witmans, N.: New insights into the geological structure of the Netherlands; results of a detailed mapping project, Netherlands Journal of Geosciences - Geologie en Mijnbouw, 91, 419–446, https://doi.org/10.1017/S0016774600000329, 2012.

Limberger, J., Boxem, T., Pluymaekers, M., Bruhn, D., Manzella, A., Calcagno, P., Beekman, F., Cloetingh, S., and van Wees, J. D. (2018). Geothermal energy in deep aquifers: A global assessment of the resource base for direct heat utilization, Renewable and Sustainable Energy Reviews, 82, 961-975, https://doi.org/10.1016/j.rser.2017.09.084, 2018.

Mart, Y. and Dauteuil, O.: Analogue experiments of propagation of oblique rifts, Tectonophysics, 316, 121–132, https://doi.org/10.1016/S0040-1951(99)00231-0, 2000.

McClay, K. R. and White, M. J.: Analogue modelling of orthogonal and oblique rifting, Mar Pet Geol, 12, 137–151, https://doi.org/10.1016/0264-8172(95)92835-K, 1995.

Michon, L., van Balen, R. T., Merle, O., and Pagnier, H.: The Cenozoic evolution of the Roer Valley Rift System integrated at a European scale, Tectonophysics, 367, 101–126, https://doi.org/10.1016/S0040-1951(03)00132-X, 2003.

Mijnlieff, H. F.: Introduction to the geothermal play and reservoir geology of the Netherlands, Netherlands Journal of Geosciences, 99, e2, https://doi.org/10.1017/njg.2020.2, 2020.

Naliboff, J. and Buiter, S. J. H.: Rift reactivation and migration during multiphase extension, Earth Planet Sci Lett, 421, 58–67, https://doi.org/10.1016/j.epsl.2015.03.050, 2015.

O'Sullivan, C. M., Childs, C. J., Saqab, M. M., Walsh, J. J., and Shannon, P. M.: Tectonostratigraphic evolution of the Slyne Basin, Solid Earth, 13, 1649–1671, https://doi.org/10.5194/se-13-1649-2022, 2022.

Peron-Pinvidic, G. and Manatschal, G.: Rifted Margins: State of the Art and Future Challenges, Front Earth Sci (Lausanne), 7, https://doi.org/10.3389/feart.2019.00218, 2019.

Racero-Baena, A. and Drake, S. J.: Structural style and reservoir development in the West Netherlands oil province, in: Geology of Gas and Oil under the Netherlands, Springer Netherlands, Dordrecht, 211–227, https://doi.org/10.1007/978-94-009-0121-6_18, 1996.

Riedel, W.: Zur Mechanik geologischer Brucherscheinungen ein Beitrag zum Problem der Fiederspatten, Centralblatt für Mineralogie, Geologie und Paläontologie, 354-368,1929.

695   Rosenbaum, G., Lister, G. S., and Duboz, C.: Relative motions of Africa, Iberia and Europe during Alpine orogeny, Tectonophysics, 359, 117-129, https://doi.org/10.1016/S0040-1951(02)00442-0, 2002.

Sanderson, D. J. and Marchini, W. R. D.: Transpression, J Struct Geol, 6, 449–458, https://doi.org/10.1016/0191-8141(84)90058-0, 1984.

700   Sissingh, W.: Palaeozoic and Mesozoic igneous activity in the Netherlands: a tectonomagmatic review, Netherlands Journal of Geosciences - Geologie en Mijnbouw, 83, 113–134, https://doi.org/10.1017/S0016774600020084, 2004.

Sylvester, A. G.: Strike-slip faults, Geol Soc Am Bull, 100, 1666–1703, https://doi.org/10.1130/0016-7606(1988)100%3C1666:SSF%3E2.3.CO;2, 1988.

705

Tari, G., Arbouille, D., Schléder, Z., and Tóth, T.: Inversion tectonics: a brief petroleum industry perspective, Solid Earth, 11, 1865-1889, https://doi.org/10.5194/se-11-1865-2020, 2020.

TNO-GDN: Stratigraphic Nomenclature of the Netherlands, https://www.dinoloket.nl/en/stratigraphic-nomenclature, last

710   access: 10 May 2023.

van der Voet, E., Heijnen, L., and Reijmer, J. J. G.: Geological evolution of the Chalk Group in the northern Dutch North Sea: inversion, sedimentation and redeposition, Geol Mag, 156, 1265–1284, https://doi.org/10.1017/S0016756818000572, 2019.

715   Voigt, T., Kley, J., and Voigt, S.: Dawn and dusk of Late Cretaceous basin inversion in central Europe, Solid Earth, 12, 1443-1471, https://doi.org/10.5194/se-12-1443-2021, 2021.

Vondrak, A. G., Donselaar, M. E., and Munsterman, D. K.: Reservoir architecture model of the Nieuwerkerk Formation (Early Cretaceous, West Netherlands Basin): diachronous development of sand-prone fluvial deposits, Geological Society, London,

720   Special Publications, 469, 423–434, https://doi.org/10.1144/SP469.18, 2018.

van Wijhe, D. H.: Structural evolution of inverted basins in the Dutch offshore, Tectonophysics, 137, 171–219, https://doi.org/10.1016/0040-1951(87)90320-9, 1987.

725   Wilcox, R. E., Harding, T. P., and Seely D. R.: Basic Wrench Tectonics, AAPG Bulletin, 57, 74-96, 1973.

Willems, C. J. L.: Doublet deployment strategies for geothermal Hot Sedimentary Aquifer exploitation: Application to the Lower Cretaceous Nieuwerkerk Formation in the West Netherlands Basin, Delft University of Technology, The Netherlands, 147 pp., 2017.

730

Willems, C. J. L. and M. Nick, H.: Towards optimisation of geothermal heat recovery: An example from the West Netherlands Basin, Appl Energy, 247, 582–593, https://doi.org/10.1016/j.apenergy.2019.04.083, 2019.

Willems, C. J. L., Nick, H. M., Donselaar, M. E., Weltje, G. J., and Bruhn, D. F.: On the connectivity anisotropy in fluvial Hot

735   Sedimentary Aquifers and its influence on geothermal doublet performance, Geothermics, 65, 222–233, https://doi.org/10.1016/j.geothermics.2016.10.002, 2017a.

Willems, C. J. L., Nick, H. M., Weltje, G. J., and Bruhn, D. F.: An evaluation of interferences in heat production from low enthalpy geothermal doublets systems, Energy, 135, 500-512, https://doi.org/10.1016/j.energy.2017.06.129, 2017b.

740

Willems, C. J. L., Vondrak, A., Munsterman, D. K., Donselaar, M. E., and Mijnlieff, H. F.: Regional geothermal aquifer architecture of the fluvial Lower Cretaceous Nieuwerkerk Formation – a palynological analysis, Netherlands Journal of Geosciences, 96, 319–330, https://doi.org/10.1017/njg.2017.23, 2017c.

745   Willems, C. J. L., Vondrak, A., Mijnlieff, H. F., Donselaar, M. E., and van Kempen, B. M. M.: Geology of the Upper Jurassic to Lower Cretaceous geothermal aquifers in the West Netherlands Basin – an overview, Netherlands Journal of Geosciences, 99, e1, https://doi.org/10.1017/njg.2020.1, 2020.

Williams, G. D., Powell, C. M., and Cooper, M. A.: Geometry and kinematics of inversion tectonics, Geological Society,

750   London, Special Publications, 44, 3–15, https://doi.org/10.1144/GSL.SP.1989.044.01.02, 1989.

Wong, T. E, Batjes, D. A. J., and de Jager, J. (Eds.): Geology of the Netherlands, Royal Netherlands Academy of Arts and Sciences, Amsterdam, The Netherlands, 362 pp., ISBN 978-9069844817, 2007.

755   Woodcock, N. H. and Fischer, M.: Strike-slip duplexes, J Struct Geol, 8, 725–735, https://doi.org/10.1016/0191-8141(86)90021-0, 1986.

Worum, G. and Michon, L.: Implications of continuous structural inversion in the West Netherlands Basin for understanding controls on Palaeogene deformation in NW Europe, J Geol Soc London, 162, 73–85, https://doi.org/10.1144/0016-764904-011, 2005.
760

Worum, G., Michon, L., van Balen, R., van Wees, J., Cloetingh, S., and Pagnier, H.: Pre-Neogene controls on present-day fault activity in the West Netherlands Basin and Roer Valley Rift System (southern Netherlands): role of variations in fault orientation in a uniform low-stress regime, Quat Sci Rev, 24, 473–488, https://doi.org/10.1016/j.quascirev.2004.02.020, 2005.

765

Ziegler, P. A.: North Sea rift system, Tectonophysics, 208, 55–75, https://doi.org/10.1016/0040-1951(92)90336-5, 1992.

Zwaan, F. and Schreurs, G.: How oblique extension and structural inheritance influence rift segment interaction: Insights from 4D analog models, Interpretation, 5, SD119–SD138, https://doi.org/10.1190/INT-2016-0063.1, 2017.

770

Zwaan, F., Schreurs, G., Naliboff, J., and Buiter, S. J. H.: Insights into the effects of oblique extension on continental rift interaction from 3D analogue and numerical models, Tectonophysics, 693, 239–260, https://doi.org/10.1016/j.tecto.2016.02.036, 2016.